

GALAXY INFALL MODELS FOR ARBITRARY VELOCITY DIRECTIONS

JENNY WAGNER ^{1,2,3} AND DAVID BENISTY  ⁴

¹*Helsinki Institute of Physics, P.O. Box 64, FI-00014 University of Helsinki, Finland, wagner@asiaa.sinica.edu.tw*

²*Academia Sinica Institute of Astronomy and Astrophysics, 11F of AS/NTU Astronomy-Mathematics Building, Roosevelt Rd, Taipei 106216, Taiwan, R.O.C*

³*Bahamas Advanced Study Institute and Conferences, 4A Ocean Heights, Hill View Circle, Stella Maris, Long Island, The Bahamas*

⁴*Leibniz-Institut für Astrophysik Potsdam (AIP), An der Sternwarte 16, 14482 Potsdam, Germany, benidav@aip.de*

ABSTRACT

For most galaxies in the cosmos, our knowledge of their motion is limited to line-of-sight velocities from redshift observations. Peculiar motions on the sky are only measured for a few cases. With increasingly detailed observations, the assumption that line-of-sight velocities suffice for an accurate and precise reconstruction of galaxy kinematics needs to be re-investigated and the impact of perpendicular velocities to be quantified. We analyse the relative motion of two galaxies with arbitrary velocities, determine the velocity between the two galaxies on an arbitrary background, and compare this general relative velocity to the one inferred from line-of-sight components only. The latter are known as “minor and major infall models” established by [Karachentsev & Kashibadze \(2006\)](#). Our derivations reveal that the infall models approximate the total radial velocity between two galaxies by two different projections employing different information about the system. For galaxies having small angular separations, all infall models agree that the radial velocity is the difference of their line-of-sight velocity components. For larger angles, the minor infall model is mostly suitable when perpendicular velocity components are negligible and there is no information about the tangential velocity of the binary system. The major infall model is best suitable when the motion is mainly radial and symmetry assumptions cancel the tangential and one perpendicular component. The latter often requires to transition from galaxy binaries to groups or clusters, as we demonstrate quantitatively. We give an encompassing overview how the infall models over- and under-estimate general binary or N -body motions. We quantify the impact of perpendicular velocity components, sparse sampling, and deviations of the tracer-galaxies from the motion in an embedding gravitational potential which are related to the angular momentum of the structure. The infall model most suitable for the kinematics reconstruction can be selected depending on available observables and supported assumptions.

Keywords: astrometry – Galaxies: kinematics and dynamics – Techniques: radial velocities – Galaxies: statistics

1. INTRODUCTION

Studying the relative motion between cosmic structures is complicated for observers like us who are located at a random external position. In the majority of cases, external observers only measure velocity components along their lines of sight to the cosmic objects. This is often done by highly precise spectroscopic redshift observations. Most objects, like galaxies, do not have a directly observable peculiar motion on the observer’s celestial sky. For instance, the peculiar motion for our neighbour-galaxy, M31, was inferred from peculiar-motion measurements of its stars and modelling its satellite dwarf galaxy motions ([Sohn et al. 2012](#); [van der Marel et al. 2012](#)).

Depending on the distance to us, spectroscopic redshifts need to be partitioned into a contribution from a cosmological background model and the velocity on top of it. The latter task is difficult in our cosmic neighbourhood, where both contributions play an equally important role, see recent observations and estimates by Cosmicflows ([Tully et al. 2023](#); [Valade et al. 2024](#)) or the Dark Energy Spectroscopic Instrument ([DESI Collaboration 2024](#); [Said et al. 2024](#)).

Reconstructing a self-consistent map of our cosmic neighbourhood of mass (density) distributions from galaxies, groups to clusters and their motions, many models have been used. Two seminal works were [Karachentsev & Kashibadze](#)

(2006) and [Karachentsev & Nasonova \(2010\)](#). They considered two limiting cases: the minor infall model assumes that galaxies are mainly moved by an expanding cosmological background, a linear Hubble flow, and are only subject to a small mutual gravitational attraction. The major infall model assumes that galaxies fall into the gravitational potential of a galaxy group or cluster instead of following the cosmic (Hubble) flow.

Both models neglect the velocity components perpendicular to the observer’s line of sight, they assume that the structure is spherically symmetric to calculate the radial infall velocity and that it is embedded in a linear Hubble flow. The authors then tried to select applications that obey these assumptions well and reduce the impact of the unknown tangential velocity component at the same time. [Karachentsev & Kashibadze \(2006\)](#) applied both models to the Local Group and the M81/M82-group, [Karachentsev & Nasonova \(2010\)](#) analysed the Virgo cluster. In ([Karachentsev & Kashibadze 2006](#)) they probed the impact of the tangential velocity by a simulation. Following-up, [Kim et al. \(2020\)](#) analysed the Hubble flow around Virgo and used minor and major infall velocities, after [Sorce et al. \(2016\)](#) only used the minor infall for a similar study.

To overcome these restrictions and to generalise the models for a deeper analytical understanding, we describe a gen-

eral binary motion without assuming spherical symmetry or specifying the embedding cosmology. Staying on this general, kinematics-only level, it remains open if the motions occur in a gravitationally bound or unbound volume. We also include the perpendicular velocity components into the models, as detailed in Section 2. For the first time, we quantify their impact on the infall models and derive conditions under which the infall models yield lower or upper bounds to the true radial infall velocity. Analogously, we investigate the role of the tangential velocity. We also compare the two infall models with each other to derive the general conditions under which both models coincide. In Section 3, we then extend the formalism to galaxy groups or clusters and investigate the impact of the statistics on the accuracy of the models for larger structures. Finally, Section 4 summarises our results and gives an outlook on the applicability of the generalised models for sky surveys and comments on the dependence of the cosmological background as well.

2. PAIRWISE INFALL MODELS

2.1. Definitions and notation

To simplify calculations, we use three-dimensional vectors in bold-font, like \mathbf{r} . Their amplitudes¹ are denoted with $|\mathbf{r}|$ and their directions in terms of unit vectors by $\hat{\mathbf{r}}$. Line-of-sight components are denoted by subscript l , while components perpendicular to the line of sight are denoted with \perp as subscript. By construction, their scalar product vanishes, $\mathbf{r}_l \cdot \mathbf{r}_\perp = 0$.

In this notation, let galaxy i at redshift z_i be at a (cosmological) distance \mathbf{r}_i , moving at a total velocity \mathbf{v}_i with respect to this observer. We partition \mathbf{v}_i into a projection along the observer's line of sight and one perpendicular to it as

$$\mathbf{v}_{li} \equiv (\mathbf{v}_i \cdot \hat{\mathbf{r}}_i) \hat{\mathbf{r}}_i = |\mathbf{v}_{li}| \hat{\mathbf{r}}_i, \quad \mathbf{v}_{\perp i} \equiv (\mathbf{v}_i \cdot \hat{\mathbf{r}}_{\perp i}) \hat{\mathbf{r}}_{\perp i} = |\mathbf{v}_{\perp i}| \hat{\mathbf{r}}_{\perp i}. \quad (1)$$

Considering arbitrary motions of two galaxies $i = 1, 2$ with distances from the observer \mathbf{r}_1 and \mathbf{r}_2 and total velocities \mathbf{v}_1 and \mathbf{v}_2 , respectively, Fig. 2.1 shows all distances, and velocity components. To split every vector in its amplitude and direction, we use $|\mathbf{r}_i| \equiv \|\mathbf{r}_i\|_2$, $i = 1, 2$ and read off Fig. 2.1 that

$$|\mathbf{r}_{21}| \equiv \left(\|\mathbf{r}_1\|_2^2 + \|\mathbf{r}_2\|_2^2 - 2 \|\mathbf{r}_1\|_2 \|\mathbf{r}_2\|_2 \cos \theta \right)^{1/2}, \quad (2)$$

$$\hat{\mathbf{r}}_{21} = \frac{\mathbf{r}_2 - \mathbf{r}_1}{|\mathbf{r}_{21}|} = \frac{|\mathbf{r}_2| \hat{\mathbf{r}}_2 - |\mathbf{r}_1| \hat{\mathbf{r}}_1}{|\mathbf{r}_{21}|} \equiv \bar{r}_2 \hat{\mathbf{r}}_2 - \bar{r}_1 \hat{\mathbf{r}}_1, \quad (3)$$

$$\hat{\mathbf{r}}_{21} = (\bar{r}_2 \cos \theta - \bar{r}_1) \hat{\mathbf{r}}_1 - \bar{r}_2 \sin \theta \hat{\mathbf{r}}_{\perp 1}, \quad (4)$$

$$= (\bar{r}_2 - \bar{r}_1 \cos \theta) \hat{\mathbf{r}}_2 - \bar{r}_1 \sin \theta \hat{\mathbf{r}}_{\perp 2}, \quad (5)$$

$$\hat{\mathbf{r}}_i \cdot \hat{\mathbf{r}}_{\perp i} = 0, \quad i = 1, 2, \quad (6)$$

$$\hat{\mathbf{r}}_1 \cdot \hat{\mathbf{r}}_2 = \hat{\mathbf{r}}_{\perp 1} \cdot \hat{\mathbf{r}}_{\perp 2} = \cos \theta, \quad (7)$$

$$\hat{\mathbf{r}}_1 \cdot \hat{\mathbf{r}}_{\perp 2} = -\hat{\mathbf{r}}_2 \cdot \hat{\mathbf{r}}_{\perp 1} = \sin \theta. \quad (8)$$

¹ Amplitudes $|\cdot|$ can be negative, while the absolute (non-negative) size of a vector is denoted as $\|\cdot\|_2$.

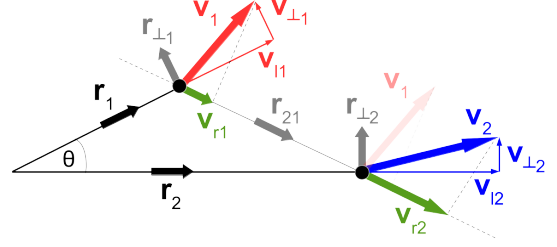


Figure 1. Three-dimensional motion of two galaxies and definition of notations. Maximum information measurable for a distant observer are velocity components along the line of sight \mathbf{v}_{li} , \mathbf{v}_{l2} to high precision via spectroscopy, highly precise angle between the galaxy positions on the sky, θ , and line-of-sight distances \mathbf{r}_1 , \mathbf{r}_2 with a precision depending on the probe used, see, Tully et al. (2023) for recent examples.

Eq. (8) can acquire a minus depending on the definition of $\mathbf{r}_{\perp i}$. Here, it follows the definition of Fig. 2.1. The directions of \mathbf{r}_i are chosen such that $|\mathbf{v}_{li}| \geq 0$ for $i = 1, 2$. There is no unique $\mathbf{r}_{\perp i}$ to \mathbf{r}_i in three dimensions. Since only \mathbf{r}_i and projections onto this vector yield observables, the non-uniqueness of $\mathbf{r}_{\perp i}$ implies that this component does not have a known direction in space. Only parts can be constrained by a projection onto the observer's sky. Due to this freedom, $\mathbf{r}_{\perp i}$ are defined such that $|\mathbf{v}_{\perp i}| \geq 0$.

Similarly, we can express the motion perpendicular to $\hat{\mathbf{r}}_{21}$. To calculate $\hat{\mathbf{r}}_{\perp 21}$, we define

$$\hat{\mathbf{n}}_1 = \bar{r}_2 \sin \theta \hat{\mathbf{r}}_1 + (\bar{r}_2 \cos \theta - \bar{r}_1) \hat{\mathbf{r}}_{\perp 1}, \quad (9)$$

$$\hat{\mathbf{n}}_2 = \bar{r}_1 \sin \theta \hat{\mathbf{r}}_2 + (\bar{r}_2 - \bar{r}_1 \cos \theta) \hat{\mathbf{r}}_{\perp 2}, \quad (10)$$

which obey $|\hat{\mathbf{n}}_i| = 1$, $\hat{\mathbf{r}}_{21} \cdot \hat{\mathbf{n}}_i = 0$, and $\hat{\mathbf{n}}_1 \cdot \hat{\mathbf{n}}_2 = 1$, $i = 1, 2$. Since $\mathbf{v}_i = \mathbf{v}_{li} + \mathbf{v}_{\perp i}$ and there is no velocity component simultaneously perpendicular to $\hat{\mathbf{r}}_i$ and $\hat{\mathbf{r}}_{\perp i}$, $\hat{\mathbf{r}}_{\perp 21} \equiv \hat{\mathbf{n}}_i$, $i = 1, 2$.

Based on these relations, we derive

$$\hat{\mathbf{r}}_1 \cdot \hat{\mathbf{r}}_{21} = \bar{r}_2 \cos \theta - \bar{r}_1, \quad (11)$$

$$\hat{\mathbf{r}}_2 \cdot \hat{\mathbf{r}}_{21} = \bar{r}_2 - \bar{r}_1 \cos \theta, \quad (12)$$

$$\hat{\mathbf{r}}_{\perp 1} \cdot \hat{\mathbf{r}}_{21} = -\bar{r}_2 \sin \theta, \quad (13)$$

$$\hat{\mathbf{r}}_{\perp 2} \cdot \hat{\mathbf{r}}_{21} = -\bar{r}_1 \sin \theta, \quad (14)$$

$$\hat{\mathbf{r}}_1 \cdot \hat{\mathbf{r}}_{\perp 21} = \bar{r}_2 \sin \theta, \quad (15)$$

$$\hat{\mathbf{r}}_2 \cdot \hat{\mathbf{r}}_{\perp 21} = \bar{r}_1 \sin \theta, \quad (16)$$

$$\hat{\mathbf{r}}_{\perp 1} \cdot \hat{\mathbf{r}}_{\perp 21} = (\bar{r}_2 \cos \theta - \bar{r}_1), \quad (17)$$

$$\hat{\mathbf{r}}_{\perp 2} \cdot \hat{\mathbf{r}}_{\perp 21} = (\bar{r}_2 - \bar{r}_1 \cos \theta). \quad (18)$$

2.2. General infall model

In the notation of Section 2.1, the relative velocity between the two galaxies reads

$$\mathbf{v}_{21} \equiv \mathbf{v}_2 - \mathbf{v}_1 = \mathbf{v}_{l2} - \mathbf{v}_{l1} + \mathbf{v}_{\perp 2} - \mathbf{v}_{\perp 1} \quad (19)$$

$$= |\mathbf{v}_{l2}| \hat{\mathbf{r}}_2 - |\mathbf{v}_{l1}| \hat{\mathbf{r}}_1 + |\mathbf{v}_{\perp 2}| \hat{\mathbf{r}}_{\perp 2} - |\mathbf{v}_{\perp 1}| \hat{\mathbf{r}}_{\perp 1}. \quad (20)$$

To infer their radial infall velocity, we project Eq. (20) onto their connection line. Using Eqs. (2) to (18), we obtain

$$|\mathbf{v}_r| \equiv (\mathbf{v}_2 - \mathbf{v}_1) \cdot \hat{\mathbf{r}}_{21} = (\mathbf{v}_{12} - \mathbf{v}_{11}) \cdot \hat{\mathbf{r}}_{21} + (\mathbf{v}_{\perp 2} - \mathbf{v}_{\perp 1}) \cdot \hat{\mathbf{r}}_{21} \quad (21)$$

$$= |\mathbf{v}_{11}| \bar{r}_1 + |\mathbf{v}_{12}| \bar{r}_2 - \cos \theta (|\mathbf{v}_{11}| \bar{r}_2 + |\mathbf{v}_{12}| \bar{r}_1) + \sin \theta (|\mathbf{v}_{\perp 1}| \bar{r}_2 - |\mathbf{v}_{\perp 2}| \bar{r}_1) . \quad (22)$$

Thus, the radial velocity is expressed via the observable quantities θ , \mathbf{r}_1 , \mathbf{r}_2 , \mathbf{v}_{11} , and \mathbf{v}_{12} and the unknown quantities $\mathbf{v}_{\perp 1}$ and $\mathbf{v}_{\perp 2}$. As a derived quantity, $|\mathbf{v}_r|$ can have negative, positive, or zero values. To linear order in θ , Eq. (22) reads

$$|\mathbf{v}_r| \approx |\mathbf{v}_{12}| - |\mathbf{v}_{11}| + \theta (|\mathbf{v}_{\perp 1}| \bar{r}_2 - |\mathbf{v}_{\perp 2}| \bar{r}_1) , \quad (23)$$

such that $|\mathbf{v}_r|$ is the difference between the line-of-sight components plus a perturbation.

Similarly, projecting Eq. (19) onto $\hat{\mathbf{r}}_{\perp 21}$, we obtain the velocity component perpendicular to the radial one

$$|\mathbf{v}_t| \equiv (\mathbf{v}_2 - \mathbf{v}_1) \cdot \hat{\mathbf{r}}_{\perp 21} \quad (24)$$

$$= (\mathbf{v}_{12} - \mathbf{v}_{11}) \cdot \hat{\mathbf{r}}_{\perp 21} + (\mathbf{v}_{\perp 2} - \mathbf{v}_{\perp 1}) \cdot \hat{\mathbf{r}}_{\perp 21} \quad (25)$$

$$= \sin \theta (|\mathbf{v}_{12}| \bar{r}_1 - |\mathbf{v}_{11}| \bar{r}_2) \quad (26)$$

$$+ |\mathbf{v}_{\perp 2}| \bar{r}_2 + |\mathbf{v}_{\perp 1}| \bar{r}_1 - \cos \theta (|\mathbf{v}_{\perp 1}| \bar{r}_2 + |\mathbf{v}_{\perp 2}| \bar{r}_1) \approx |\mathbf{v}_{\perp 2}| - |\mathbf{v}_{\perp 1}| + \theta (|\mathbf{v}_{12}| \bar{r}_1 - |\mathbf{v}_{11}| \bar{r}_2) . \quad (27)$$

We denote this component the tangential velocity. As a derived quantity, it can have any negative, positive, or zero value. To leading order, $|\mathbf{v}_t|$ is proportional to the difference of the perpendicular velocity components plus a perturbation.

We can also express the velocity difference as a combination of radial and tangential components

$$\mathbf{v}_2 - \mathbf{v}_1 \equiv \mathbf{v}_r + \mathbf{v}_t = |\mathbf{v}_r| \hat{\mathbf{r}}_{21} + |\mathbf{v}_t| \hat{\mathbf{r}}_{\perp 21} . \quad (28)$$

Since \mathbf{v}_t is not observable in general, we read off Eq. (26), under which conditions $|\mathbf{v}_t| = 0$. For arbitrary θ , we obtain the general relation between the unknown and known quantities

$$|\mathbf{v}_{\perp 1}| + |\mathbf{v}_{\perp 2}| \frac{\bar{r}_2 - \bar{r}_1 \cos \theta}{\bar{r}_1 - \bar{r}_2 \cos \theta} = \frac{\sin \theta (|\mathbf{v}_{12}| \bar{r}_1 - |\mathbf{v}_{11}| \bar{r}_2)}{\bar{r}_2 \cos \theta - \bar{r}_1} . \quad (29)$$

Two special cases are

$$\theta = 0 \wedge |\mathbf{v}_{\perp 1}| = |\mathbf{v}_{\perp 2}| , \quad (30)$$

$$|\mathbf{v}_{\perp 1}| = |\mathbf{v}_{\perp 2}| \frac{\bar{r}_2 - \bar{r}_1 \cos \theta}{\bar{r}_2 \cos \theta - \bar{r}_1} \wedge \bar{r}_2 |\mathbf{v}_{11}| = \bar{r}_1 |\mathbf{v}_{12}| . \quad (31)$$

Thus, the conditions for a purely radial infall are fine-tuned relative velocity components. The cases stated in prior work like Eq. (30) within the measurement precision thus greatly depend on additional assumptions, like spherical symmetry, to achieve the fine-tuning. Only selecting galaxies almost aligned on the observer's line of sight is not sufficient to achieve $|\mathbf{v}_t| = 0$.

Assuming the perpendicular velocity components are unknown in Eq. (22), we find that the last term containing these

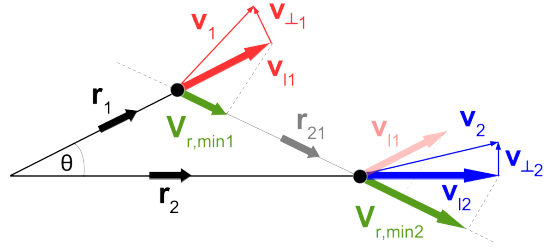


Figure 2. Minor infall model: the line-of-sight velocity components of both galaxies are projected onto their connection line. The difference of these projections yields the relative radial velocity.

components vanishes for $\theta \neq 0$ and $|\mathbf{r}_i| \neq 0$ if

$$|\mathbf{v}_{\perp 1}| \bar{r}_2 = |\mathbf{v}_{\perp 2}| \bar{r}_1 \Leftrightarrow \left(\frac{|\mathbf{v}_{\perp 1}|}{|\mathbf{v}_{\perp 2}|} = \frac{|\mathbf{r}_1|}{|\mathbf{r}_2|} \right) \vee (\mathbf{v}_{\perp 1} = \mathbf{v}_{\perp 2} = 0) . \quad (32)$$

These insights have an important impact on the minor and major infall models as discussed below.

2.3. Minor infall - projection on the connection line

In this infall model, originally defined to describe the motion of two galaxies whose velocities are dominated by their surrounding Hubble flow, $|\mathbf{v}_{li}| \gg |\mathbf{v}_{\perp i}|$, their relative radial velocity is

$$|\mathbf{v}_{r,\min}| \equiv (\mathbf{v}_{12} - \mathbf{v}_{11}) \cdot \hat{\mathbf{r}}_{21} \quad (33)$$

$$= |\mathbf{v}_{11}| \bar{r}_1 + |\mathbf{v}_{12}| \bar{r}_2 - \cos \theta (|\mathbf{v}_{11}| \bar{r}_2 + |\mathbf{v}_{12}| \bar{r}_1) , \quad (34)$$

which neglects the last term in Eq. (22). Fig. 2.3 visualises the situation. For $\theta \neq 0$ and $|\mathbf{r}_i| \neq 0$, we find that the minor infall model is a good approximation to the true radial velocity, if one of the two options in Eq. (32) holds. We also read off Eqs. (22) and (34) that, for $0 < \theta < \pi$, $|\mathbf{v}_r|$ is under-estimated by Eq. (34) if $|\mathbf{v}_{\perp 1}| / |\mathbf{v}_{\perp 2}| > |\mathbf{r}_1| / |\mathbf{r}_2|$. Vice versa, $|\mathbf{v}_r|$ is over-estimated by Eq. (34) if $|\mathbf{v}_{\perp 1}| / |\mathbf{v}_{\perp 2}| < |\mathbf{r}_1| / |\mathbf{r}_2|$.

For $\mathbf{v}_i \approx \mathbf{v}_{li}$, $i = 1, 2$, meaning $\mathbf{v}_{\perp i} \approx 0$, we find that Eq. (26) is reduced to the first term which consists of observable quantities up to the unknown direction of $\hat{\mathbf{r}}_{\perp 21}$. So it is impossible to calculate \mathbf{v}_t in general, which explains why the minor infall model does not make a statement about it. At best, we can exploit $\sin \theta \in [-1; 1]$ for $\mathbf{v}_i \approx \mathbf{v}_{li}$ to constrain $|\mathbf{v}_t|$ by

$$- (|\mathbf{v}_{12}| \bar{r}_1 - |\mathbf{v}_{11}| \bar{r}_2) \leq |\mathbf{v}_t| \leq + (|\mathbf{v}_{12}| \bar{r}_1 - |\mathbf{v}_{11}| \bar{r}_2) . \quad (35)$$

2.4. Major infall - projection on one line of sight

We first employ this infall model for two galaxies. Yet, we already note that the original approach replaced galaxy 2 by the centre of mass of a galaxy group and considered the infall of a galaxy onto the centre instead of a binary motion (see Section 3).

Shown in Fig. 2.4, the major infall model determines the radial velocity of galaxy 1 with respect to galaxy 2 by projecting all relevant velocity components onto $\hat{\mathbf{r}}_1$

$$|\mathbf{v}_{r,\text{maj}}| \hat{\mathbf{r}}_{21} \cdot \hat{\mathbf{r}}_1 = (\mathbf{v}_{12} - \mathbf{v}_{11}) \cdot \hat{\mathbf{r}}_1 , \quad (36)$$

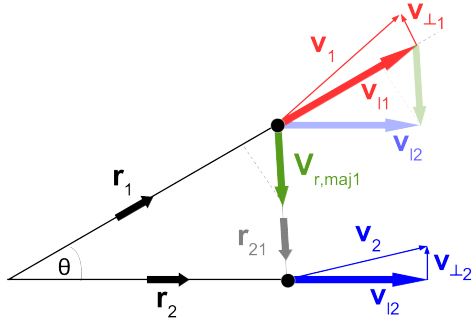


Figure 3. Major infall model for galaxy 1: the radial infall velocity of galaxy 1 onto galaxy 2 is determined from the projection of the radial infall velocity and the line-of-sight velocity of galaxy 2 onto the line-of-sight of galaxy 1. An analogous procedure yields the major infall model for galaxy 2. Due to the asymmetry of this model, both radial infall velocities need not be of the same size.

analogously for galaxy 2. Solving for $|v_{r,\text{maj}i}|$ for $i = 1, 2$, yields

$$|v_{r,\text{maj}1}| = \frac{|v_{12}| \cos \theta - |v_{11}|}{\bar{r}_2 \cos \theta - \bar{r}_1}, \quad (37)$$

$$|v_{r,\text{maj}2}| = \frac{|v_{11}| \cos \theta - |v_{12}|}{\bar{r}_2 - \bar{r}_1 \cos \theta}. \quad (38)$$

For comparison, the generalised version of the major infall model is obtained by projecting Eq. (28) onto \hat{r}_i

$$(\mathbf{v}_2 - \mathbf{v}_1) \cdot \hat{r}_i = (|v_r| \hat{r}_{21} + |v_t| \hat{r}_{\perp 21}) \cdot \hat{r}_i, \quad i = 1, 2. \quad (39)$$

Solving for $|v_r|$, we obtain

$$|v_r| = \frac{|v_{12}| \cos \theta - |v_{11}| + \sin \theta (|v_{\perp 2}| - \bar{r}_2 |v_t|)}{(\bar{r}_2 \cos \theta - \bar{r}_1)}, \quad i = 1 \quad (40)$$

$$\approx |v_{12}| - |v_{11}| + \theta (|v_{\perp 2}| - \bar{r}_2 |v_t|), \quad (41)$$

$$|v_r| = \frac{|v_{12}| - |v_{11}| \cos \theta + \sin \theta (|v_{\perp 1}| - \bar{r}_1 |v_t|)}{(\bar{r}_2 - \bar{r}_1 \cos \theta)}, \quad i = 2 \quad (42)$$

$$\approx |v_{12}| - |v_{11}| + \theta (|v_{\perp 1}| - \bar{r}_1 |v_t|). \quad (43)$$

Thus, the major infall model is accurate for $\theta \neq 0$ and $\mathbf{r}_i \neq 0$ if

$$i = 1 : |v_{\perp 2}| = \bar{r}_2 |v_t|, \quad \text{or} \quad i = 2 : |v_{\perp 1}| = \bar{r}_1 |v_t|. \quad (44)$$

Combining both equations to eliminate the unknown $|v_t|$ yields Eq. (32) again. So, the conditions for over- or under-estimation of the true radial velocity are the same as for the minor infall.

A special case is $|v_t| = 0$, implying a purely radial infall, and $|v_{\perp i}| = 0$, $i = 1, 2$. Only considering one equation of Eqs. (40) and (42), this case yields a purely radial infall of one galaxy under a symmetry constraint that forces the perpendicular velocity of the other galaxy or the group centre to vanish (see Section 3).

2.5. Comparison and limits

The general versions of the infall models are easily related to each other via the different projections and it is obvious that both models are independent of a background cosmology. The minor infall model is best used when we do not have more information beyond θ , v_{li} , $i = 1, 2$. Since the model does not make any assumption about v_t and treats each galaxy of a pair equally, it is well-suited to describe binary galaxies.

In contrast, the major infall model is best used for an ensemble of several galaxies. While it can also describe a pair, it requires information about the tangential and perpendicular components. The latter can be added via symmetry assumptions, readily testable in groups but hard to establish for binaries.

Replacing galaxy 2 by the centre of mass of the entire structure, explains why the major infall model is asymmetric in the infalling objects. Any external impact, like an accelerated cosmic expansion, will not generate additional angular momentum, increasing $v_{\perp 2}$. Symmetry assumptions and a correspondingly well-sampled distribution of galaxies then allow us to describe groups and clusters robustly even over cosmic time.

Comparing Eqs. (34) and (37), or (38), their difference reads

$$|v_{r,\text{min}}| - |v_{r,\text{maj}1}| = (|v_{12}| - |v_{11}|) \left(1 - \frac{\bar{r}_1 + 1}{\bar{r}_2} \frac{|v_{12}| \cos \theta - |v_{11}|}{|v_{12}| - |v_{11}|} \right) \quad (45)$$

and analogously for $|v_{r,\text{maj}2}|$. For $\mathbf{r}_i \neq 0$ and $v_{12} \neq v_{11}$, the infall models only agree for $\theta = 0$. Thus, only for small angles, as considered in prior work, both models coincide in the trivial relation up to small deviations

$$|v_{r,\text{min}}| = |v_{r,\text{maj}1}| = |v_{r,\text{maj}2}| = |v_r| = |v_{12}| - |v_{11}|. \quad (46)$$

For $0 < \theta < \pi$, the second term on the right-hand side of Eq. (45) is negative, such that $|v_{r,\text{min}}| - |v_{r,\text{maj}1}| > 0$ if $|v_{12}| - |v_{11}| > 0$. Yet, since both models over- or under-estimate the true radial infall velocity based on Eq. (32), we cannot decide which model is closer to the true radial component without additional information or assumptions.

3. FROM BINARIES TO GROUPS AND CLUSTERS

The approaches in Karachentsev & Kashibadze (2006) rely on spherical symmetry and require the member galaxies to sample the total spherical mass distribution well. To investigate the impact of each assumption, let the centre of the *total* mass distribution (stellar, gaseous, dark mass) be \mathbf{r}_{cm} and its total velocity $v_{\text{cm}} = d\mathbf{r}_{\text{cm}}/dt$. For n member galaxies sampling this mass-density profile, their centre of mass and its velocity are given by

$$\mathbf{r}_{\text{cg}} = \frac{1}{M_g} \sum_{i=1}^n m_i \mathbf{r}_i, \quad \mathbf{v}_{\text{cg}} = \frac{1}{M_g} \sum_{i=1}^n m_i \mathbf{v}_i, \quad (47)$$

where M_g is the mass of all galaxies and we assumed that the galaxies move non-relativistically. While M_g is known when

the mass-to-light ratio of the galaxies is known, the total mass of the structure M remains unknown, for instance, including a galaxy-cluster-scale dark-matter halo in which the galaxies are moving, so $M \geq M_g$. The galaxies are a representative sample if, at least, $\mathbf{r}_{\text{cm}} = \mathbf{r}_{\text{cg}}$ and $\mathbf{v}_{\text{cm}} = \mathbf{v}_{\text{cg}}$. These quantities need not agree generally, for instance, for a very small number of galaxies, in merger scenarios, or if the dark matter distribution is not well-traced by the luminous matter. For $\mathbf{r}_i = \mathbf{r}_{\text{cm}} - \mathbf{r}_{\text{cm}i}$ and $\mathbf{v}_i = \mathbf{v}_{\text{cm}} - \mathbf{v}_{\text{cm}i}$, the total momentum with respect to the observer is

$$\mathbf{P} = M_g \mathbf{v}_{\text{cm}} - \sum_{i=1}^n m_i \mathbf{v}_{\text{cm}i}. \quad (48)$$

If $\mathbf{r}_{\text{cm}} = \mathbf{r}_{\text{cg}}$, the sum vanishes. Assuming a spherically symmetric structure on a homogeneous and isotropic background, \mathbf{v}_{cm} reduces to the cosmic velocity along the observer's line of sight. Without these assumptions, \mathbf{P} is not well-constrained even for $n \gg 2$ due to the unknown perpendicular and tangential parts.

The total angular momentum with respect to the observer is

$$\mathbf{L} = \sum_{i=1}^n m_i \mathbf{r}_i \times \mathbf{v}_i \equiv |\mathbf{L}_1 + \mathbf{L}_2 - \mathbf{L}_3 - \mathbf{L}_4| \hat{\mathbf{r}}_{\text{cm}} \times \hat{\mathbf{r}}_{\perp\text{cm}}. \quad (49)$$

With the relations in Section 2.1, the four parts read

$$|\mathbf{L}_1| = \left| \sum_{i=1}^n m_i \mathbf{r}_{\text{cm}} \times \mathbf{v}_{\perp\text{cm}} \right| = M_g |\mathbf{r}_{\text{cm}}| |\mathbf{v}_{\perp\text{cm}}|, \quad (50)$$

$$|\mathbf{L}_2| = \left| \sum_{i=1}^n m_i \mathbf{r}_{\text{cm}i} \times \mathbf{v}_{\perp\text{cm}i} \right| = \sum_{i=1}^n m_i |\mathbf{r}_{\text{cm}i}| |\mathbf{v}_{\text{ti}}|, \quad (51)$$

$$|\mathbf{L}_3| = \left| \sum_{i=1}^n m_i \mathbf{r}_{\text{cm}i} \times \mathbf{v}_{\text{cm}} \right|, \quad (52)$$

$$= \sum_{i=1}^n m_i (|\mathbf{v}_{\perp\text{cm}}| (|\mathbf{r}_{\text{cm}}| - |\mathbf{r}_i| \cos \theta_i) + |\mathbf{v}_{\text{cm}}| |\mathbf{r}_i| \sin \theta_i) \quad (53)$$

$$|\mathbf{L}_4| = \left| \sum_{i=1}^n m_i \mathbf{r}_{\text{cm}} \times \mathbf{v}_{\text{cm}i} \right| = - \sum_{i=1}^n m_i |\mathbf{v}_{\text{ri}}| |\mathbf{r}_{\text{cm}}| \bar{r}_i \sin \theta_i. \quad (54)$$

For an arbitrary observer in a homogeneous and isotropic universe, there is no reason for a total angular momentum to exist, such that $|\mathbf{L}| = 0$ for an isolated single structure, supported by observations Hawking (1969); Saadeh et al. (2016). As assumed in Karachentsev & Kashibadze (2006), if $\mathbf{r}_{\text{cm}} = \mathbf{r}_{\text{cg}}$, \mathbf{L}_3 and \mathbf{L}_4 vanish. From the remaining $|\mathbf{L}_1| = -|\mathbf{L}_2|$, we obtain

$$|\mathbf{v}_{\perp\text{cm}}| + \frac{m_j}{M_g} \frac{|\mathbf{r}_{\text{cm}j}|}{|\mathbf{r}_{\text{cm}}|} |\mathbf{v}_{\text{ti}}| = - \sum_{i=1, i \neq j}^n \frac{m_i}{M_g} \frac{|\mathbf{r}_{\text{cm}i}|}{|\mathbf{r}_{\text{cm}}|} |\mathbf{v}_{\text{ti}}|, \quad (55)$$

taking galaxy j outside the sum, assuming it falls onto a structure of $n - 1$ galaxies. Then, we require $n \gg 1$ and

a spherically symmetric structure in which the right-hand side of Eq. (55) averages to zero. Eq. (55) amounts to $|\mathbf{v}_{\perp\text{cm}}| = \lambda \bar{r}_{\text{cm}} |\mathbf{v}_{\text{ti}}|$ compared to Eq. (44). However, only the projection of \mathbf{v}_{ti} on the observer's sky can be observed. So we may absorb λ into the definition of \mathbf{v}_{ti} for the infall model and study its degeneracies with the projection angle on the observer's sky in a subsequent step. The major infall model then relates $|\mathbf{v}_{\text{ti}}|$ to $|\mathbf{v}_{\perp\text{cm}}|$.

Alternatively, all galaxies are in the spherically symmetric structure on the right-hand side of Eq. (55), hence $|\mathbf{v}_{\perp\text{cm}}| = 0$. Inserting the latter into Eqs. (40) and (42), solving for $|\mathbf{v}_{\perp i}|$ and $|\mathbf{v}_{\text{ti}}|$ yields

$$|\mathbf{v}_{\perp i}| = 0 \quad \vee \quad \theta = 0 \quad \vee \quad \theta = \pi/2 \quad \vee \quad \theta = \pi. \quad (56)$$

Hence, the $|\mathbf{v}_{\text{ti}}|$ do not need to vanish, so that the minor infall model is equally suitable to be used in this case.

The trivial case $|\mathbf{v}_{\perp\text{cm}}| = |\mathbf{v}_{\text{ti}}| = 0$ mentioned in Section 2.4 is obtained for a purely radial infall, $|\mathbf{v}_{\text{ti}}| = 0$ either for galaxy j onto a spherical structure, or even $\forall j = 1, \dots, n$, both yielding $|\mathbf{L}_1| = |\mathbf{L}_2| = 0$. Deviations from Eq. (44) can already arise from $|\mathbf{L}_2|$ due to a less symmetric structure or insufficient sampling n , apart from asymmetries between \mathbf{r}_{cm} and \mathbf{r}_{cg} causing \mathbf{L}_3 and \mathbf{L}_4 to be non-zero.

Rewriting Eq. (49) in terms of all $|\mathbf{v}_{\text{r,maj}i}|$, we use Eq. (40) with a λ -factor in front of $|\mathbf{v}_{\text{ti}}|$ as above but without the mass ratio, and $\theta_i \neq 0$ to obtain

$$|\mathbf{L}_1 + \mathbf{L}_2| = \sum_{i=1}^n \frac{m_i}{\sin \theta_i} |\mathbf{r}_{\text{cm}}| (\bar{r}_{\text{cm}} \cos \theta_i - \bar{r}_i) (|\mathbf{v}_{\text{ri}}| - |\mathbf{v}_{\text{r,maj}i}|). \quad (57)$$

For $\theta_i = 0$, Eq. (46) holds without giving a contribution to Eq. (57). Detailed in Section 2.4, the major infall model may over- or under-estimate $|\mathbf{v}_{\text{r}|}$, such that any $|\mathbf{L}| \neq 0$ depends on the sum of deviations for all galaxies, which, in turn, depends on the symmetry of the structure. Since the minor infall does not include $|\mathbf{v}_{\text{ti}}|$, Eq. (57) only relates the major infall model to the true radial velocity.

4. CONCLUSIONS

We described an arbitrary binary motion on a general background including the velocity components perpendicular to the observer's lines of sight and the tangential velocity. In doing so, we generalised the radial infall models of Karachentsev & Kashibadze (2006) that predict the relative velocity between pairs of galaxies or a galaxy falling towards the centre of mass of a group or cluster using the observed line-of-sight velocity components only.

Both models are just different approximations to the general description when different information is available, as summarised in Fig. 4: For galaxies having small angular separations, all infall models agree that their relative radial velocity is the difference of their line-of-sight velocity components, Eq. (46). The M81-M82 binary system from Karachentsev & Kashibadze (2006), which will be revisited in Benisty et al. (2025), is such an example. For arbitrary angles, we derived how the original models under- or overestimate the true radial velocity depending on the distance

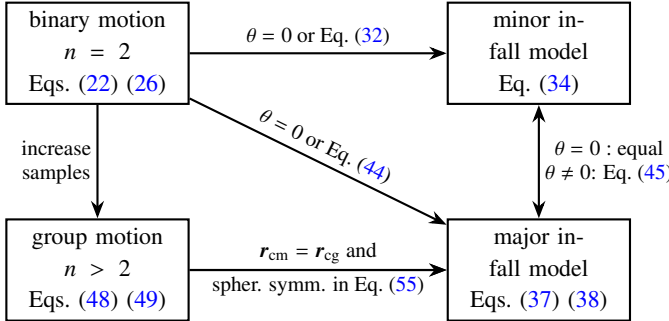


Figure 4. Summary of all results: conditions to apply the infall models, their formulae, relations, and accuracy.

ratio, Eq. (32). This extends the findings of Kim et al. (2020) why minor and major infall models yield different H_0 -values and that the true radial velocity need not be between the ones inferred from both models. In Eq. (45), we also show that the difference between the two infall models can be larger or smaller than zero depending on the difference between the line-of-sight velocities.

The symmetric minor infall model is mostly suitable when perpendicular velocity components are negligible and there

is no information about the tangential velocity, like binary galaxies.

The asymmetric major infall model is best suitable when the motion is mainly radial and symmetry assumptions allow us to cancel the tangential and one perpendicular component. The latter requires a transition from binaries to groups or clusters, one exception being our Local Group, for which respective observables are available (Benisty et al. 2022). With SDSS- and DESI-redshifts available, galaxy clusters like Virgo (Kim et al. 2020) with about $n = 1000$ member galaxies are suitable test-beds.

We also show fine-tuned conditions under which the infall models are accurate and which may apply to individual cases. Specifying the background as our concordance cosmology, it is more likely that perpendicular and tangential velocities vanish for a statistics of systems. So, tests for the Cosmological Principle, as detailed in Aluri et al. (2023), may be refined.

Quantifying the impact of so-far unobserved velocity components on cosmic structure reconstruction will be useful when those components are observed. But it is already helpful to explain and motivate the infall models and tighten the constraints on the radial velocities.

DB is supported by a Minerva Fellowship of the Minerva Stiftung Gesellschaft für die Forschung mbH.

REFERENCES

Aluri, P. k., Cea, P., Chingangbam, P., et al. 2023, Classical and Quantum Gravity, 40, 094001, doi: [10.1088/1361-6382/acbefc](https://doi.org/10.1088/1361-6382/acbefc)

Benisty, D., Libeskind, N. I., & Hoffman, Y. 2025, in prep.

Benisty, D., Vasiliev, E., Evans, N. W., et al. 2022, ApJL, 928, L5, doi: [10.3847/2041-8213/ac5c42](https://doi.org/10.3847/2041-8213/ac5c42)

DESI Collaboration. 2024, AJ, 168, 58, doi: [10.3847/1538-3881/ad3217](https://doi.org/10.3847/1538-3881/ad3217)

Hawking, S. 1969, MNRAS, 142, 129, doi: [10.1093/mnras/142.2.129](https://doi.org/10.1093/mnras/142.2.129)

Karachentsev, I. D., & Kashibadze, O. G. 2006, Astrophysics, 49, 3, doi: [10.1007/s10511-006-0002-6](https://doi.org/10.1007/s10511-006-0002-6)

Karachentsev, I. D., & Nasonova, O. G. 2010, MNRAS, 405, 1075, doi: [10.1111/j.1365-2966.2010.16501.x](https://doi.org/10.1111/j.1365-2966.2010.16501.x)

Kim, Y. J., Kang, J., Lee, M. G., & Jang, I. S. 2020, ApJ, 905, 104, doi: [10.3847/1538-4357/abbd97](https://doi.org/10.3847/1538-4357/abbd97)

Saadeh, D., Feeney, S. M., Pontzen, A., Peiris, H. V., & McEwen, J. D. 2016, PhRvL, 117, 131302, doi: [10.1103/PhysRevLett.117.131302](https://doi.org/10.1103/PhysRevLett.117.131302)

Said, K., Howlett, C., Davis, T., et al. 2024, arXiv e-prints, arXiv:2408.13842, doi: [10.48550/arXiv.2408.13842](https://doi.org/10.48550/arXiv.2408.13842)

Sohn, S. T., Anderson, J., & van der Marel, R. P. 2012, ApJ, 753, 7, doi: [10.1088/0004-637X/753/1/7](https://doi.org/10.1088/0004-637X/753/1/7)

Sorce, J. G., Gottlöber, S., Hoffman, Y., & Yepes, G. 2016, MNRAS, 460, 2015, doi: [10.1093/mnras/stw1085](https://doi.org/10.1093/mnras/stw1085)

Tully, R. B., Kourkchi, E., Courtois, H. M., et al. 2023, ApJ, 944, 94, doi: [10.3847/1538-4357/ac94d8](https://doi.org/10.3847/1538-4357/ac94d8)

Valade, A., Libeskind, N. I., Pomarède, D., et al. 2024, Nature Astronomy, doi: [10.1038/s41550-024-02370-0](https://doi.org/10.1038/s41550-024-02370-0)

van der Marel, R. P., Fardal, M., Besla, G., et al. 2012, ApJ, 753, 8, doi: [10.1088/0004-637X/753/1/8](https://doi.org/10.1088/0004-637X/753/1/8)